Heterobimetallic Systems Containing Organometallic and Classical Coordination Sites: Effects of Subtle Changes in the Werner-Type Site

Tianlu Sheng,[a] Sebastian Dechert,[a] A. Claudia Stückl,[a] and Franc Meyer*[a]

Keywords: Bridging ligands / Cyclopentadienyl ligands / Heterometallic complexes / N ligands / Manganese / Zinc

Several highly unsymmetrical heterodinuclear Mn/Zn complexes are reported, in which an organometallic $CpMn(CO)_2$ fragment and a classical Werner-type zinc coordination unit are arranged in close proximity by means of a bridging pyrazolate. Ligand scaffolds differing in the chelate size of the tripodal tetradentate $\{N_4\}$ binding site, and different co-ligands for zinc are employed. Both the zinc-devoid precursor compounds and the bimetallic complexes with zinc(II) nested in the tris(pyridylalkyl)amine type $\{N_4\}$ compartment have been characterized by X-ray crystallography. Structural and spectroscopic features as well as the redox potentials of the Mn^I/Mn^{II} couple indicate slight effects of the redox-inactive Werner-type subunit on the properties of the organometallic site. Oxidation is highly localized at the organometallic manganese site, as is evidenced by IR and EPR spectroscopy and supported by DFT calculations.

Introduction

Complexes of cyclopentadienyl (Cp) ligands bearing functional amino or amido side-chains are currently receiving enormous attention in organometallic chemistry.[1,2] While the donor substituent tethered to the Cp moiety might serve an intramolecular function, for example acting as a (sometimes hemilabile) chelate donor in generic type **A** complexes (Scheme 1),[3,4] it may also serve an intermolecular function, for example by anchoring to a solid support or providing solubility.[3] A further possibility is the introduction of a potentially bridging moiety that will lead to highly preorganized bimetallic systems formally composed of a type **A** Cp∩N fragment and an adjacent second metal ion. In this respect we have recently developed a synthetic approach for the construction of type **B** bimetallic complexes where a pyrazolate group linking two Cp units functions both as an intramolecular N-donor and as a bridging unit spanning two metals.[5,6] The dimanganese complex **1** has been studied in detail and has been shown to undergo two sequential, one-electron, metal-centered oxidations with fast intramolecular thermal-electron transfer ($k_{ET} \approx 2.6\times10^{10}\ s^{-1}$ at 298 K) in the mixed-valent Mn^IMn^{II} species.[6] In an extension of this concept, a first access to highly unsymmetrical heterobimetallic type **D** scaffolds has recently been developed.[7] These can be formally viewed as a combination of one type **A** and one type **C** subunit, i.e. as an assembly of both a Werner-type and an organometallic fragment in a preorganized bimetallic array. This description is corroborated by the structural characterization of the only such complex reported to date (**2**),[7] since inspection of its individual subunits reveals close similarities to related mononuclear complexes. In particular, the zinc subunit of **2** is reminiscent of the well-known $[(tmpa)ZnCl]^+$ complex, where tmpa is tripodal tetradentate tris(pyridylmethyl)amine. Oxidation of **2** occurs at around –0.66 V (versus the ferrocene couple), and IR spectroscopic evidence showed it to be Mn-centered.[7]

These findings suggest to probe type **D** systems in metal-mediated reactions that proceed by coordination of substrates to the M^2 metal ion in the classical Werner-type site, with the $CpMn(CO)_2$ subunit serving as an electron reservoir, but without direct involvement of the manganese in substrate binding. In the case of redox-active metal ions in the $\{N_4\}$ site, this approach may lead to well-defined systems capable of novel "one-site-addition-two-metal-oxidation" reactions.[8] Two characteristics of type **D** complexes are noteworthy in this regard: firstly, the rigid chelate arrangement precludes dissociation of the organometallic fragment from the bridging pyrazolate, and secondly, the π plane of the heterocycle roughly coincides with the mirror plane of the $Mn(CO)_2$ moiety. The latter situation is most favorable for Mn-pyrazolate π-interactions and hence for electronic communication between the Mn site and the second metal ion.[6,9,10]

It seems particularly attractive that type **D** compounds offer the potential to introduce various different ligand environments for the Werner-type coordination site. Fundamental to an understanding of bimetallic chemistry of those complexes is the knowledge of how different Werner-type

[a] Institut für Anorganische Chemie, Georg-August-Universität Göttingen,
Tammanstraße 4, 37077 Göttingen, Germany
Fax: +49-551-393063
E-mail: franc.meyer@chemie.uni-goettingen.de
Supporting information for this article is available on the WWW under http://www.eurjic.org or from the author.

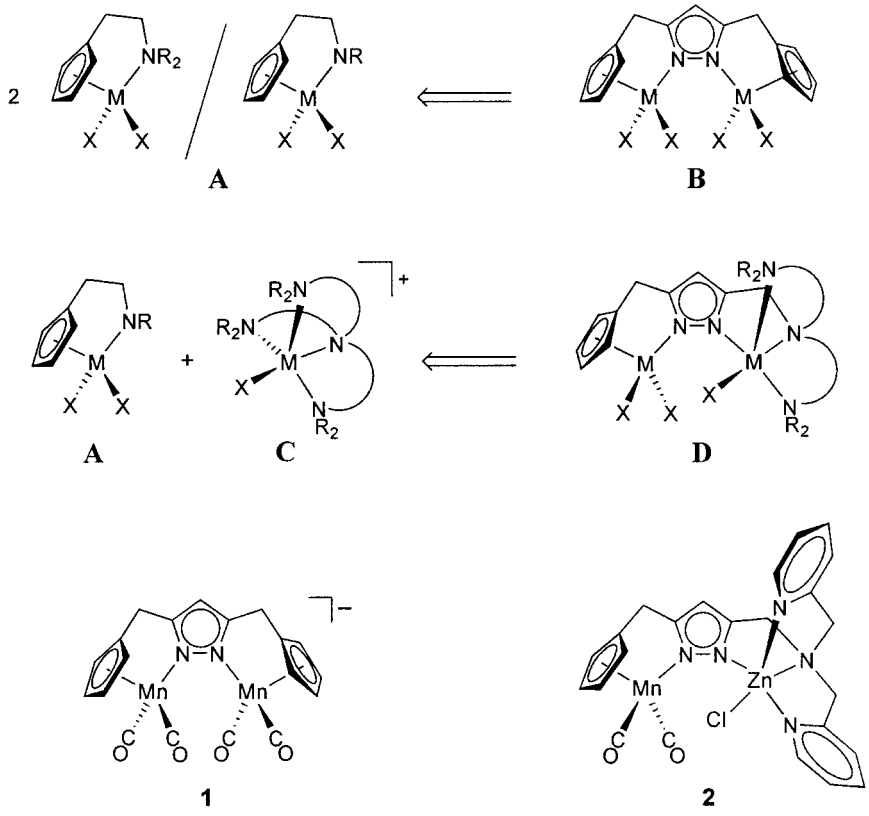

Scheme 1.

sites influence the properties of the redox-active $CpMn(CO)_2$ subunit, even in the absence of any M^2 or in the case of a redox-inactive M^2 ion such as zinc(II). The present contribution now reports two (Cp∩pyrazolate)$Mn(CO)_2$ systems with different chain lengths in the bis(pyridylalkyl) amine side-arms and several zinc complexes thereof. Effects of the different ligand side-arms and different anionic co-ligands (either coordinating or noncoordinating) on structural and electrochemical properties are investigated.

Results and Discussion

Synthesis and Structural Characterization of Complexes

The synthesis of pyrazole derivative **5a** with appended cyclopentadienyltricarbonylmanganese and bis(pyridylmethyl)amine substituents has been communicated previously and had been used for the direct synthesis of **2**.[7] Following the same synthetic strategy we have now prepared the analogous compound **5b** with a longer bis(pyridylethyl)amine side-arm (Scheme 2).

Starting from **3**, which is readily available in five steps from 3,5-dimethylpyrazole,[5,11] the $CpMn(CO)_3$ moiety was first introduced in a palladium-catalyzed cross-coupling reaction and the bis(pyridylmethyl)amine arm was subsequently attached to give 2-tetrahydropyranyl (thp)-protected **5b**. The thp group was then removed under acidic conditions. Irradiation of **5a**,**b** leads to elimination of one CO and intramolecular coordination of the pyrazole-N.[12] This reaction can be conveniently followed by IR spectroscopy. The resulting complexes **6a**,**b** were isolated and fully characterized, including by X-ray crystallography. Their molecular structures are depicted in Figure 1 and Figure 2, respectively, together with selected atom distances and bond angles.

The geometric parameters for the $CpMn(CO)_2$ fragments of **6a**,**b** are very similar to those of **1** and **2** reported previously.[6,7] The proton bound to the pyrazole-N(2) is involved in hydrogen bonding to the N-atoms of the pendent pyridine side-arms. Interestingly, it forms an intramolecular hydrogen bond in the case of **6b** [d{N(2)···N(5)} = 2.977(2) Å; Figure 2], while intermolecular hydrogen bonding that leads to a polymeric chain structure in the solid state is observed for **6a** [d{N(2)···N(5′)} = 2.825(2) Å; Figure 3]. Involvement of the pyrazole-NH in H-bonding has recently also been found to be crucial for unidentate pyrazole coordination.[13]

Heterobimetallic complexes with zinc ions in the $\{N_4\}$ donor compartment are best prepared in a one-pot procedure starting from **5a**,**b**. Thus, solutions of **6a**,**b** prepared in situ were treated with one equivalent of KO*t*Bu and one equivalent of $Zn(OAc)_2{\cdot}2H_2O$. Single crystals of **7a**·DMF·H_2O and **7b** (Scheme 3) were finally obtained by slow diffusion of Et_2O into DMF or CH_2Cl_2 solutions of the products, respectively. The constitution of both complexes was elucidated by X-ray crystallography. Molecular

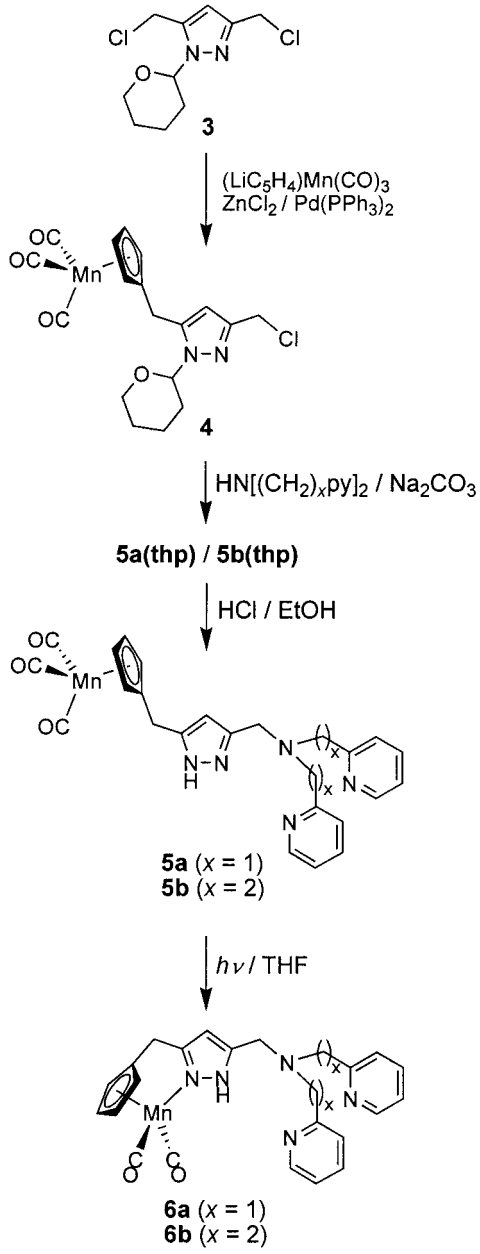

Scheme 2. Synthesis of **6a** and **6b**.

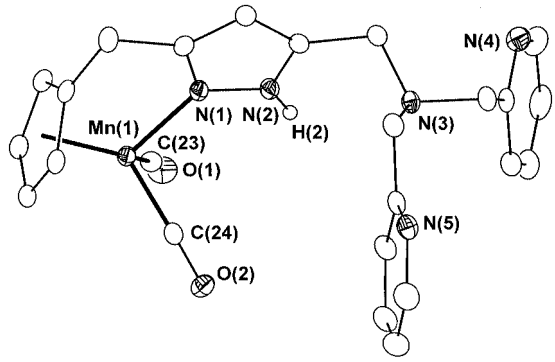

Figure 1. ORTEP plot (30% probability thermal ellipsoids) of the structure of **6a**. For the sake of clarity all hydrogen atoms, except H(2), have been omitted. Selected atom distances [Å] and angles [°] [Cg(1) defines the centroid of the Cp ring atoms]: Mn(1)–Cg(1) 1.7686(9), Mn(1)–N(1) 2.006(2), Mn(1)–C(23) 1.772(2), Mn(1)–C(24) 1.771(2), C(23)–O(1) 1.167(2), C(24)–O(2) 1.162(2); Cg(1)–Mn(1)–N(1) 111.24(5), Cg(1)–Mn(1)–C(23) 125.84(7), Cg(1)–Mn(1)–C(24) 125.04(7), C(23)–Mn(1)–C(24) 90.81(9), C(23)–Mn(1)–N(1) 102.15(8), C(23)–Mn(1)–N(1) 95.98(7), O(1)–C(23)–Mn(1) 173.5(2), O(2)–C(24)–Mn(1) 178.2(2).

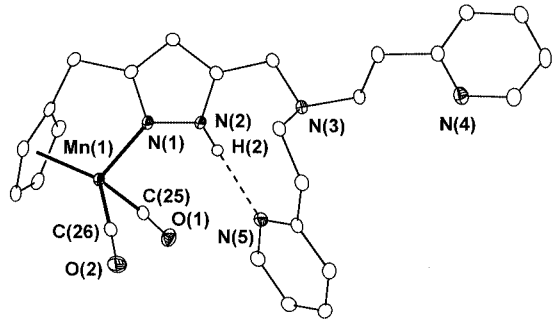

Figure 2. ORTEP plot (30% probability thermal ellipsoids) of the molecular structure of **6b**. For the sake of clarity all hydrogen atoms, except H(2), have been omitted. Selected atom distances [Å] and angles [°] [Cg(1) defines the centroid of the Cp ring atoms]: Mn(1)–Cg(1) 1.772(1), Mn(1)–N(1) 2.020(2), Mn(1)–C(25) 1.767(2), Mn(1)–C(26) 1.775(2), C(25)–O(1) 1.165(3), C(26)–O(2) 1.163(3); Cg(1)–Mn(1)–N(1) 111.16(6), Cg(1)–Mn(1)–C(25) 123.87(8), Cg(1)–Mn(1)–C(26) 127.21(8), C(25)–Mn(1)–C(26) 89.4(1), C(25)–Mn(1)–N(1) 100.45(8), C(26)–Mn(1)–N(1) 99.29(8), O(1)–C(25)–Mn(1) 174.8(2), O(2)–C(26)–Mn(1) 176.2(2); N(2)–H(2) 0.83(3), H(2)···N(5) 2.15(3), N(2)···N(5) 2.977(2); N(2)–H(2)···N(5) 170(2).

structures are depicted in Figure 4 and Figure 5, respectively, together with selected atom distances and bond angles.

The zinc ions in both **7a** and **7b** are nested in the classical $\{N_4\}$ coordination site and the pyrazolate bridge spans the $CpMn(CO)_2$ fragment and the zinc(II), as anticipated. Due to the rigid chelating ligand framework, the N(1)–Mn–CO bond angles of all complexes studied in this work are somewhat widened [95.2(1)–103.1(1)°]. A CSD search revealed that complexes of $CpMn(CO)_2$ fragments with N-donor ligands not tethered to the Cp usually have N–Mn–CO bond angles in the range 92.6–99.4°.

In **7a**, the zinc is five-coordinate with the bridgehead-N(3) and the carboxylate-O(3) in the apical positions of a distorted trigonal bipyramid [N(3)–Zn(1)–O(3) = 170.2(1)°; τ = 0.77].[14] This situation closely resembles the molecular structure of the mononuclear zinc benzoate complex of tmpa.[15] The remaining O(4) atom of the acetate in **7a** is involved in hydrogen bonding to a water molecule included in the crystal lattice (the water is further hydrogen bonded to a DMF solvent molecule; see Figure S1 in the Supporting Information). In contrast, the acetate ligand in **7b** adopts a semi-bidentate binding mode with one short and one significantly longer Zn–O bond [d\{Zn(1)–O(3)\} = 2.049(3) Å, d\{Zn(1)–O(4)\} = 2.447(2) Å]. This is accompanied by an increase in the metal–metal separation [d\{Mn(1)–Zn(1)\} = 4.1423(9) Å in **7a** versus d\{Mn(1)–Zn(1)\} = 4.3915(6) Å in **7b**] and a more drastic displacement of the metal ions out of the plane of the pyrazolate.

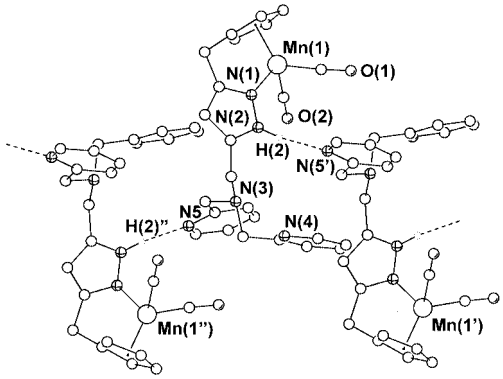

Figure 3. View of the hydrogen-bond structure of **6a**. Selected atom distances [Å] and angles [°]: N(2)–H(2) 0.90(2), H(2)···N(5′) 1.96(2), N(2)···N(5′) 2.825(2); N(2)–H(2)···N(5′) 161(2). Symmetry transformation used to generate equivalent atoms (′): 3/2 – *x*, *y* – 1/2, –*z* + 1/2.

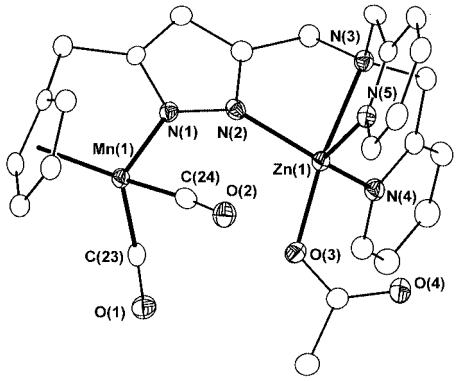

Figure 4. ORTEP plot (30% probability thermal ellipsoids) of the molecular structure of **7a**. For the sake of clarity all hydrogen atoms have been omitted. Selected atom distances [Å] and angles [°] [Cg(1) defines the centroid of the Cp ring atoms]: Mn(1)–Cg(1) 1.773(2), Mn(1)–N(1) 2.026(3), Mn(1)–C(23) 1.768(4), Mn(1)–C(24) 1.760(4), Mn(1)···Zn(1) 4.1423(9), Zn(1)–O(3) 1.947(3), Zn(1)–N(2) 2.008(3), Zn(1)–N(3) 2.312(3), Zn(1)–N(4) 2.143(3), Zn(1)–N(5) 2.074(3), O(1)–C(23) 1.166(5), O(2)–C(24) 1.185(4); Cg(1)–Mn(1)–N(1) 111.5(1), Cg(1)–Mn(1)–C(23) 125.3(2), Cg(1)–Mn(1)–C(24) 123.6(1), C(23)–Mn(1)–C(24) 90.3(2), C(23)–Mn(1)–N(1) 99.8(2), C(24)–Mn(1)–N(1) 101.4(2), O(1)–C(23)–Mn(1) 175.4(4), O(2)–C(24)–Mn(1) 172.8(3), N(2)–Zn(1)–N(3) 78.3(1), N(2)–Zn(1)–N(4) 111.3(1), N(2)–Zn(1)–N(5) 108.8(1), N(2)–Zn(1)–O(3) 108.0(1), N(3)–Zn(1)–N(4) 74.6(1), N(3)–Zn(1)–N(5) 77.1(1), N(3)–Zn(1)–O(3) 170.2(1), N(4)–Zn(1)–N(5) 124.0(1), N(4)–Zn(1)–O(3) 96.0(1), N(5)–Zn(1)–O(3) 107.1(1).

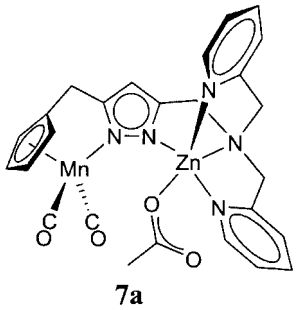

7a

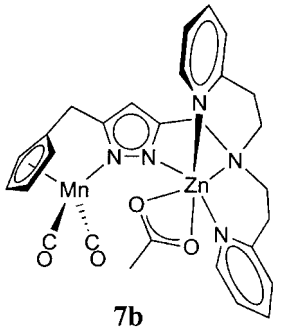

7b

Scheme 3. Heterobimetallic Mn/Zn complexes.

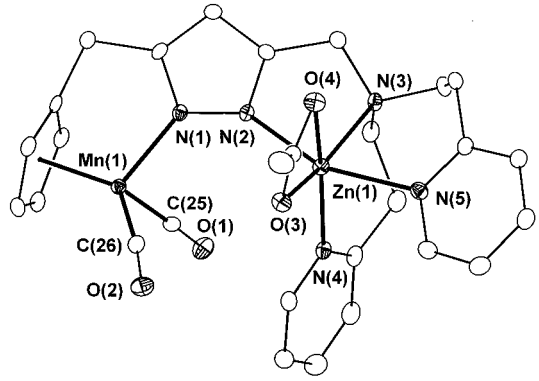

Figure 5. ORTEP plot (30% probability thermal ellipsoids) of the molecular structure of **7b**. For the sake of clarity all hydrogen atoms have been omitted. Selected atom distances [Å] and angles [°] [Cg(1) defines the centroid of the Cp ring atoms]: Mn(1)–Cg(1) 1.767(2), Mn(1)–N(1) 2.034(2), Mn(1)–C(25) 1.771(3), Mn(1)–C(26) 1.764(3), Mn(1)···Zn(1) 4.3915(6), Zn(1)–O(3) 2.049(2), Zn(1)–O(4) 2.447(2), Zn(1)–N(2) 2.088(2), Zn(1)–N(3) 2.176(2), Zn(1)–N(4) 2.068(2), Zn(1)–N(5) 2.290(3), O(1)–C(25) 1.160(4), O(2)–C(26) 1.174(4); Cg(1)–Mn(1)–N(1) 112.48(9), Cg(1)–Mn(1)–C(25) 122.4(1), Cg(1)–Mn(1)–C(26) 125.0(1), C(25)–Mn(1)–C(26) 93.2(1), C(25)–Mn(1)–N(1) 95.2(1), C(26)–Mn(1)–N(1) 103.1(1), O(1)–C(25)–Mn(1) 175.5(3), O(2)–C(26)–Mn(1) 172.7(3), N(2)–Zn(1)–N(3) 78.21(9), N(2)–Zn(1)–N(4) 103.0(1), N(2)–Zn(1)–N(5) 160.16(9), N(2)–Zn(1)–O(3) 105.18(9), N(2)–Zn(1)–O(4) 91.98(9), N(3)–Zn(1)–N(4) 99.97(9), N(3)–Zn(1)–N(5) 86.03(9), N(3)–Zn(1)–O(3) 158.66(9), N(3)–Zn(1)–O(4) 101.35(8), N(4)–Zn(1)–N(5) 91.4(1), N(4)–Zn(1)–O(3) 99.72(9), N(4)–Zn(1)–O(4) 156.03(9), N(5)–Zn(1)–O(3) 85.32(9), N(5)–Zn(1)–O(4) 79.27(9), O(3)–Zn(1)–O(4) 57.82(8).

Apparently, the six-membered chelate rings leave more space for anion coordination and allow for greater flexibility of the zinc coordination sphere. The different acetate binding modes are also discernible in the IR spectra, where **7a** features a high-energy $\nu_{as}(CO_2^-)$ vibration at $\tilde{\nu}$ = 1663 cm^{-1}, while $\nu_{as}(CO_2^-)$ of **7b** occurs around $\tilde{\nu}$ = 1607 cm^{-1}. The $\nu_s(CO_2^-)$ absorptions (expected around $\tilde{\nu}$ = 1400 cm^{-1})[16] cannot be clearly identified because of various other bands in that region.

The only known mononuclear zinc(II) complex of tris(pyridylethyl)amine (tpea), which provides longer alkyl spacers than tpma, is [(tpea)Zn](ClO$_4$)$_2$.[17] In contrast to the related zinc(II) complexes of tpma, however, the cationic portion of [(tpea)Zn](ClO$_4$)$_2$ contains four-coordinate zinc while the perchlorate remains uncoordinated. A similar sit-

uation is now found in the heterobimetallic complex **8**, which was obtained from **6b** and $[Zn(H_2O)_6](ClO_4)_2$. The molecular structure of the cation of **8** is depicted in Figure 6, together with selected atom distances and bond angles.

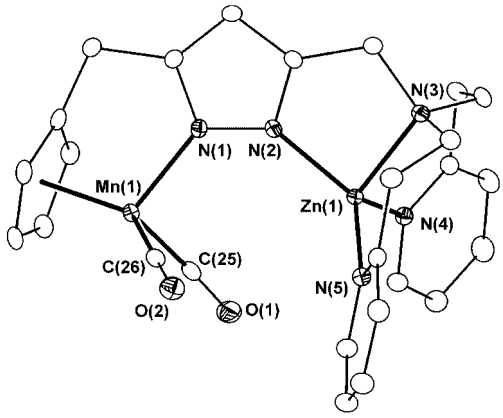

Figure 6. ORTEP plot (30% probability thermal ellipsoids) of the molecular structure of **8**. In the interests of clarity all hydrogen atoms and the ClO_4^- anion have been omitted. Selected atomic distances [Å] and angles [°] [Cg(1) defines the centroid of the Cp ring atoms]: Mn(1)–Cg(1) 1.773(1), Mn(1)–N(1) 1.991(2), Mn(1)–C(25) 1.761(3), Mn(1)–C(26) 1.774(3), Mn(1)···Zn(1) 4.0601(5), Zn(1)–N(2) 1.941(2), Zn(1)–N(3) 2.079(2), Zn(1)–N(4) 1.999(2), Zn(1)–N(5) 2.002(2), O(1)–C(25) 1.167(3), O(2)–C(26) 1.168(3); Cg(1)–Mn(1)–N(1) 110.81(7), Cg(1)–Mn(1)–C(25) 126.29(9), Cg(1)–Mn(1)–C(26) 128.3(1), C(25)–Mn(1)–C(26) 90.5(1), C(25)–Mn(1)–N(1) 99.16(9), C(26)–Mn(1)–N(1) 94.62(9), O(1)–C(25)–Mn(1) 177.2(2), O(2)–C(26)–Mn(1) 179.5(2), N(2)–Zn(1)–N(3) 85.24(8), N(2)–Zn(1)–N(4) 124.58(8), N(2)–Zn(1)–N(5) 114.46(8), N(3)–Zn(1)–N(4) 101.93(8), N(3)–Zn(1)–N(5) 103.88(8), N(4)–Zn(1)–N(5) 116.61(8).

The coordination geometry of Zn(1) in **8** is distorted tetrahedral, the strongest distortion resulting from the presence of an acute angle in the five-membered chelate ring [N(2)–Zn(1)–N(3) = 85.24(8)°]. Both the zinc and the manganese ions are located roughly within the plane of the pyrazolate heterocycle [out-of-plane displacement: 0.317(1) Å for Zn and 0.269(1) Å for Mn], indicating a relaxed bonding situation. The closest distance between Zn(1) and a CO ligand is almost 3.5 Å, which is clearly out of the bonding range.[18] Due to the absence of any coordinating counteranion, the Mn···Zn distance [4.0601(5) Å] is clearly shorter than in **7b**. Comparison of the structures of **7b** and **8** reveals that binding of small substrate molecules to the zinc ion in **8** should be feasible.

Spectroscopic and Electrochemical Trends

Incorporation of zinc in the $\{N_4\}$ compartment of **6a**,**b** to give **7a**,**b** induces a slight shift of the ν(CO) stretching frequencies to lower wavenumbers (Table 1; spectra of KBr pellets), thereby indicating an increase in π-backbonding from the manganese ion to the CO ligands. This is also reflected by a slight decrease of the $Mn–C_{CO}$ distance (mean value for **6a**,**b**: 1.771 Å; mean value for **7a**,**b**: 1.766 Å) and a slight increase of the C–O distance (mean value for **6a**,**b**: 1.164 Å; mean value for **7a**,**b**: 1.171 Å). The effects are less pronounced for **8**, which can be ascribed to the cationic charge of its MnZn entity. While mainly located at zinc, to a small extent the electronic unsaturation in **8** is apparently transmitted also towards the manganese.

Table 1. IR absorptions in the CO stretching range, along with *g* values and isotropic coupling constants derived from EPR spectra of the oxidized species.

	DMF solution [cm^{-1}]		KBr pellets [cm^{-1}]		g_{iso}	$a(^{55}Mn)_{iso}$ [mT]
6a	1915	1841	1910	1827	–	–
6a$^+$	2020	1934	–	–	2.036	6.10
6b	1913	1841	1912	1838	–	–
6b$^+$	2021	1935	–	–	2.038	6.04
7a	1910	1837	1901	1831	–	–
7a$^+$	2029	1950	–	–	2.044	6.16
7b	1914	1840	1898	1823	–	–
7b$^+$	2021	1935	–	–	2.040	6.17
8	1913	1838	1906	1833	–	–
8$^+$	2021	1935	–	–	–	–

The higher electron density at the manganese ions in **7a**,**b** should correspond to a more facile oxidation of manganese(I) in the heterobimetallic complexes than for the zinc-devoid precursors, which was confirmed by cyclic voltammograms of **6a**,**b** and **7a**,**b** (the cyclic voltammogram of **7a** is shown in Figure 7 as an example). The zinc-devoid compounds exhibit a reversible, one-electron oxidation wave at around $E_{1/2}$ = –0.35 V (versus the ferrocene/ferrocenium couple), while oxidation of the heterobimetallic complexes occurs around $E_{1/2}$ = –0.60 V (Table 2). This shift to more negative potentials is probably due to the higher electron-donating power of the ligand towards manganese as a consequence of the deprotonation of the pyrazole. In accordance with the spectroscopic results discussed above, the electron-poor **8** is clearly more difficult to oxidize than the corresponding acetate complex **7b** with a potential intermediate between those of **6b** and **7b** (the redox process is only quasi-reversible in the case of **8**).

The oxidation potentials of $CpMn(CO)_2L$ complexes are known to vary over a potential range of more than 2 V, depending on the nature of the ligand L.[9,10,19] The rather low oxidation potentials of **6a**,**b** and **7a**,**b** indicate significant stabilization of the Mn^{II} state by the anionic pyrazolate ligand and reflect the high nucleophilicity of the N-heterocycle, in particular in the heterobimetallic species.[19] However, a considerable cathodic shift is observed upon binding of the zinc ions. Zinc itself is redox inactive, but comparison of **7a** and **7b** reveals that the different Werner-type coordination subunits do indeed influence the redox properties of the $CpMn(CO)_2$ group, even though the effects are only minor (difference in $E_{1/2}$ of about 30 mV between **7a** and **7b**). Also, a certain degree of information about the type of coligand at zinc is transmitted to manganese, resulting in slight shifts in the Mn^I/Mn^{II} redox potential (**7b** versus **8**).

Chemical oxidation with $[Cp_2Fe]PF_6$ in DMF solution allowed the IR spectroscopic determination of the ν(CO) absorptions of the oxidized species (Table 1, Figure 8).

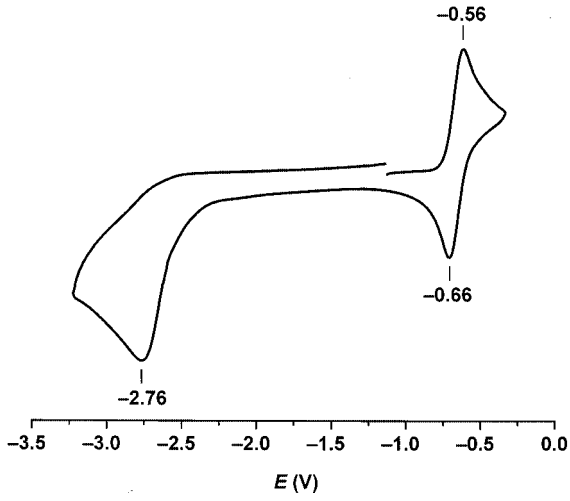

Figure 7. Cyclic voltammogram of **7a** in DMF. Potentials are given in volts versus the ferrocen/ferrocenium couple.

Table 2. Formal potentials for the Mn^{II}/Mn^{I} couple in DMF/0.1 M Bu_4NPF_6. Values are given in volts versus Fc/Fc^+.

6a	–0.33
6b	–0.35
7a	–0.61
7b	–0.58
8	–0.44 (quasi rev.)

Within minutes at room temperature, however, these bands gradually vanished without concomitant rise of any new bands in the CO stretching region, thus indicating irreversible decomposition of the oxidized $Mn^{II}Zn^{II}$ complexes. Solution EPR spectra at this point show an isotropic six-line signal around g = 2.009 with $a(^{55}Mn)_{iso}$ = 9.43 mT, suggesting extrusion of the manganese(II) ions and formation of $[Mn(DMF)_6]^{2+}$.[20] Unambiguous EPR characterization of the oxidized Mn^{II} (**6a**$^+$, **6b**$^+$) and $Mn^{II}Zn^{II}$ species (**7a**$^+$, **7b**$^+$, **8**$^+$) after chemical oxidation with $[Cp_2Fe]PF_6$ in a THF/DMF mixture was hampered by the immediate formation of a dominant signal for the $[Mn(DMF)_6]^{2+}$ decomposition product. In CH_2Cl_2 the product of decomposition seems to form less rapidly and is insoluble, which allows EPR spectroscopic characterization of the oxidized species (**6a**$^+$, **6b**$^+$, **7a**$^+$, **7b**$^+$) in solution. All EPR spectra after chemical oxidation with a substoichiometric amount of $[Cp_2Fe]PF_6$ in CH_2Cl_2 solution show a six-line pattern with only slightly differing g values around 2.040 and isotropic coupling constants around 6.12 mT (Table 1; the spectrum of **6b**$^+$ is shown in Figure 9 as an example). The magnitude of $a(^{55}Mn)_{iso}$ is typical for a $[CpMn^{II}(CO)_2L]^+$ species and suggest that the unpaired electron is mainly localized at the manganese atom, in accordance with electronic-structure calculations (see below). The spectrum of a frozen solution of **6b**$^+$ (Figure 9) compares well with those of other $[CpMn^{II}(CO)_2L]^+$ compounds with approximate axial symmetry of the g tensor and anisotropic hyperfine coupling to a single ^{55}Mn nucleus.[21] However, decomposition of the oxidized species occurred after a few minutes at room temperature. The product of decomposition in CH_2Cl_2 shows a very broad unstructured signal centered around g = 1.994. No EPR spectrum of the oxidized $Mn^{II}Zn^{II}$ species **8**$^+$ could be recorded because of the poor solubility of **8** in CH_2Cl_2.

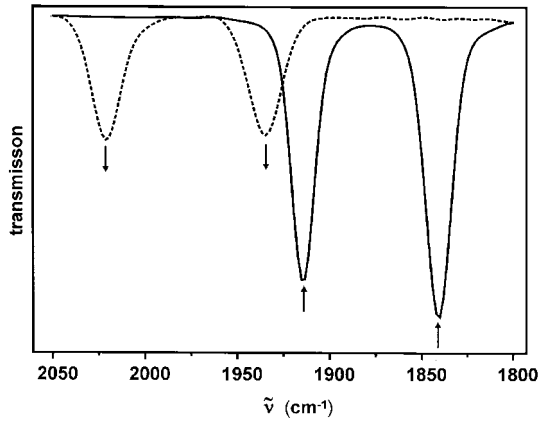

Figure 8. Stretching frequencies ν(CO) of **6b** (solid line) and after oxidation with $[Cp_2Fe]PF_6$ (**6b**$^+$, dashed line) in DMF.

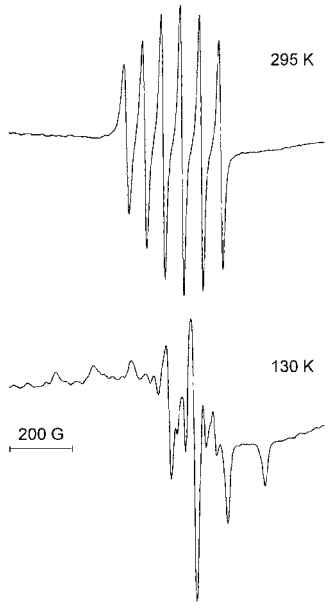

Figure 9. EPR spectra of **6b**$^+$ in CH_2Cl_2 at 295 and 130 K.

Since structural information about the oxidized species is not available, and in order to corroborate the spectroscopic findings, DFT calculations[22] were carried out for the doublet state of **8**$^+$. The geometry was DFT-minimized starting from the X-ray structure atomic coordinates for **8** to give the geometric information listed in Figure 10. The $Mn–N^{pz}$ and $Mn–C_{C\equiv O}$ bonds in **8**$^+$ were calculated to be 1.95 and 1.84 Å, respectively, which is clearly longer than the corresponding values of the $Mn^{I}Zn^{II}$ complex **8**. At the same time, the C–O distances of the Mn-bound carbonyls are significantly shortened at 1.15 Å, in agreement with diminished π-backbonding in the oxidized species and the observed shift of the IR stretching vibrations. The SOMO of **8**$^+$ is depicted in Figure 10, from which it is apparent that

the SOMO has predominant Mn 3d character with some antibonding admixture from the π-pyrazolate system.

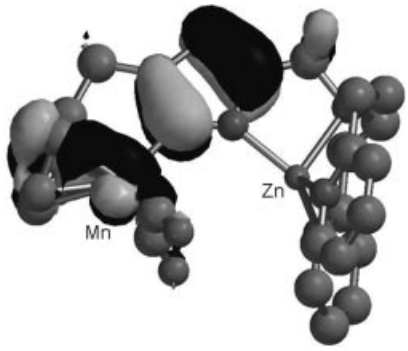

Figure 10. Calculated shape of the SOMO of **8**$^{+}$ (DFT, Spartan 02, UB3LYP/LACVP*). Selected structural parameters: Mn–N^{pz} 1.95 Å; Mn–$C_{C\equiv O}$ 1.84 Å; C–O 1.15 Å; Zn–N^{pz} 2.03 Å; Mn–N–N 139.2°; $C_{C\equiv O}$–Mn–N 98.1/98.2°; Zn–N–N 139.2°.

According to a Mulliken population analysis the spin is almost perfectly localized on manganese (ρMn = 1.017), while spin density on the pyrazolate-N is found to be negligible (ρN^{pz} = 0.009/–0.013), in accordance with the lack of any ^{55}Mn–^{14}N hyperfine coupling in the EPR spectra.

Conclusions

Highly unsymmetrical heterodinuclear Mn/Zn type **D** complexes based on a bridging pyrazolate with variable ligand environments for the classical Werner-type coordination site are accessible by the versatile synthetic approach outlined in Scheme 2. Structural characteristic of the two metal-containing subunits of the systems studied here are reminiscent of their corresponding mononuclear analogues, which supports the description of the present type **D** systems as hybrids of an organometallic $CpMn(CO)_2$ fragment and a classical Werner-type tris(pyridylalkyl)amine type $\{N_4\}$ metal site. Oxidation is highly localized at the organometallic manganese site, as is evidenced by IR and EPR spectroscopy and supported by DFT calculations. However, slight effects of the redox-inactive, Werner-type subunit of the Mn^{I}/Mn^{II} redox properties and of spectroscopic signatures of the organometallic site are revealed by comparing the zinc-devoid manganese compounds and the bimetallic Mn/Zn complexes, as well as by assessing the influence of the chelate size of the tripodal tetradentate $\{N_4\}$ binding site and of different coligands at zinc. Future work will focus on bimetallic type **D** complexes with a second redox-active metal ion other than zinc. It is hoped that application of the principles delineated in this work will allow modulation of the relative redox properties of the two distinct metal sites, and as a consequence will enable a tuning of the bimetallic redox reactivity of the "one-site-addition-two-metal-oxidation" type.

Experimental Section

General Remarks: All reagents were obtained from commercial sources (Aldrich, Fluka, or VWR) and used as received. Compounds **3**, **4**, and **5a** (Scheme 2) were prepared according to the literature methods.[5,7] Solvents were dried under reflux (CaH_2 for dichloromethane, Na/K alloy for diethyl ether and THF) and distilled prior to be used. All reactions were carried out under nitrogen using standard Schlenk techniques. IR spectra were recorded with a Digilab Excalibur, UV/Vis/NIR spectra with a Cary 5000, EPR spectra with a Bruker ELEXSYS 500. Cyclic voltammetry was performed with a potentiostat/galvanostat Perkin–Elmer Model 263A instrument with glassy-carbon working electrode and platinum reference and counter electrodes, in 0.1 M tetra-*n*-butylammonium hexafluorophosphate/DMF. Ferrocene (the potential being 0.45 V in DMF against SCE)[23] was used as internal standard. Elemental analyses were measured by the analytical laboratory of the Institut für Anorganische Chemie der Universität Göttingen using a Heraeus CHN-O-RAPID instrument.

Complex 5b(thp): Na_2CO_3 (4.0 g, 37 mmol) was dried at 100 °C under vacuum for 1 h. After cooling to room temperature, a solution of **4** (1.50 g, 3.60 mmol) and bis[2-(2-pyridyl)ethyl]amine (1.13 g, 3.80 mmol) in MeCN (100 mL) was added. The suspension was stirred overnight at 75 °C in the dark, then filtered and the residue washed several times with small portions of MeCN. Evaporation of the combined organic phases produced a red-brown oil that was purified by Kugelrohr distillation under vacuum to remove all volatile impurities and to give **5b(thp)** (yield 1.62 g, 89%). ^{1}H NMR ($CDCl_3$): δ = 1.55–1.66 (m, 3 H, CH_2^{thp}), 1.92 (d, J = 12.3 Hz, 1 H, CH_2^{thp}), 2.09 (br. s, 1 H, CH_2^{thp}), 2.41 (m, 1 H, CH_2^{thp}), 2.94 (s, 8 H, $PyCH_2CH_2N$), 3.61 (s, 2 H, CH_2Cp), 3.74 (s, 2 H, $PzCH_2$), 3.98 (d, J = 11.0 Hz, 1 H, CH_2^{thp}), 4.63 (d, J = 6.2 Hz, 2 H, CH^{Cp}), 4.69 (s, 2 H, CH^{Cp}), 5.21 (d, J = 8.7 Hz, 1 H, $CH^{thp,2}$), 5.87 (s, 1 H, $CH^{pz,4}$), 7.06 (br. s, 4 H, $CH^{py,3/5}$), 7.49 (t, J = 7.1 Hz, 2 H, $CH^{py,4}$), 8.46 (s, 2 H, $CH^{py,6}$) ppm; NH not observed. ^{13}C NMR ($CDCl_3$): δ = 22.4 ($CH_2^{thp,4}$), 24.3, 24.7 ($CH_2^{thp,5}$, CH_2Cp), 29.3 ($CH_2^{thp,3}$), 35.7 (NCH_2), 51.0, 53.5 ($PzCH_2$, $PyCH_2$), 67.2 ($CH_2^{thp,6}$), 81.4, 81.7, 83.1, 83.2 (CH^{Cp}), 84.4 ($CH^{thp,2}$), 101.9 (C^{Cp}), 106.1 ($CH^{pz,4}$), 120.6 ($CH^{py,5}$), 123.1 ($CH^{py,3}$), 135.7 ($CH^{py,4}$), 141.2 ($C^{pz,5}$), 148.8 ($CH^{py,6}$), 149.6 ($C^{pz,3}$), 160.6 ($C^{py,2}$), 224.6 (CO) ppm. MS (ESI): m/z (%) = 608 (50) [M^+], 501 (100) [M^+ – $pyCH_2CH_3$], 439 (80) [M^+ – 3CO – THP]. $C_{32}H_{34}MnN_5O_4$ (607.59): calcd. C 63.26, H 5.64, N 11.53; found C 62.86, H 5.82, N 11.34.

Complex 5b: A solution of **5b(thp)** (1.62 g, 2.67 mmol) in EtOH (20 mL) was treated with ethanolic HCl (10 mL) and stirred overnight in the dark. Addition of Et_2O (100 mL) caused precipitation of the hydrochloride salt of **5b** as a brownish solid. This was separated by filtration, neutralized with aqueous Na_2CO_3, and extracted with several portions of CH_2Cl_2. After drying the combined organic phases with $MgSO_4$, the solvent was evaporated to give the crude product as a red-brown oil that was purified by Kugelrohr distillation under vacuum to remove all volatile impurities (yield 1.28 g, 91.6%). ^{1}H NMR ($CDCl_3$): δ = 2.89 (br. s, 4 H, CH_2N), 2.99 (br. s, 4 H, $PyCH_2$), 3.59 (s, 2 H, CH_2Cp), 3.83 (br. s, 2 H, $PzCH_2$), 4.59 (s, 2 H, CH^{Cp}), 4.71 (s, 2 H, CH^{Cp}), 5.95 (br. s, 1 H, $CH^{pz,4}$), 6.97 (m, 2 H, $CH^{py,3}$), 7.07 (m, 2 H, $CH^{py,5}$), 7.51 (t, J = 7.2 Hz, 2 H, $CH^{py,4}$), 8.48 (s, 2 H, $CH^{py,6}$) ppm; NH not observed. ^{13}C NMR ($CDCl_3$): δ = 27.2, (CH_2Cp), 35.4 (NCH_2), 49.5 ($PzCH_2$), 54.0 ($PyCH_2$), 81.6, 83.2 (CH^{Cp}), 102.8 (br., $CH^{pz,4}$), 104.7 (C^{Cp}), 121.3 ($CH^{py,5}$), 123.5 ($CH^{py,3}$), 136.5 ($CH^{py,4}$), 148.9 ($CH^{py,6}$), 159.7 ($CH^{py,2}$), 225.1 (CO) ppm; $C^{pz,3/5}$ not observed. MS (ESI): m/z (%) = 524 (100) [M^+], 439 (43) [M^+ – 3CO – 1] 439. $C_{27}H_{26}MnN_5O_3$ (523.47): calcd. C 61.95, H 5.01, N 13.38; found C 62.78, H 5.36, N 13.14.

Complex 6a: A solution of **5a** (0.25 g, 0.50 mmol) in THF (200 mL) was irradiated with a high-pressure mercury lamp in a quartz tube

at –40 °C. Within about 1 h the color of the solution had changed from light yellow to yellow. The solution was allowed to warm to room temperature and the solvent was removed under reduced pressure. The residue was extracted with 10 mL of CH_2Cl_2 and filtered. Slow diffusion of Et_2O into the red solution gradually gave red crystals of the product **6a** (yield 73 mg, 31%). IR (KBr): $\tilde{\nu}$ = 3060 w, 2920 w, 2849 w, 1910 vs, 1827 vs, 1592 m, 1571 m, 1474 m, 1435 m, 1231 m, 771 m, 657 m, 612 m, 585 m cm^{-1}. $C_{24}H_{22}MnN_5O_2 \cdot 0.5\,H_2O$ (476.42): calcd. C 60.51, H 4.65, N 14.70; found C 60.56, H 4.77, N 14.58.

Complex 6b: A solution of **5b** (0.26 g, 0.50 mmol) in THF (200 mL) was irradiated with a high-pressure mercury lamp in a quartz tube at –40 °C. After about 1 h the color of the solution had changed from light yellow to yellow. The solution was allowed to warm to room temperature and the solvent was removed under vacuum. The residue was extracted with 10 mL of CH_2Cl_2 and filtered. Slow diffusion of Et_2O into the red solution gradually gave red crystals of **6b**, which were filtered, washed with Et_2O, and dried under vacuum (yield 85 mg, 34%). IR (KBr): $\tilde{\nu}$ = 3127 w, 3061 w, 2968 w, 2851 w, 1912 vs, 1838 vs, 1595 m, 1568 m, 1465 m, 1433 m, 1352 m, 1260 m, 827 m, 803 m, 758 m, 658 m, 610 m, 590 m, 507 w, 472 w cm^{-1}. $C_{26}H_{26}MnN_5O_2$ (495.46): calcd. C 63.03, H 5.29, N 14.13; found C 62.69, H 5.41, N 14.23.

Complex 7a: A solution of **5a** (0.25 g, 0.50 mmol) in THF (200 mL) was irradiated with a high-pressure mercury lamp in a quartz tube at –40 °C. After about 1 h the color of the solution had changed from light yellow to yellow, and the solution was allowed to warm to room temperature. KO*t*Bu (0.056 g, 0.50 mmol) and Zn(OAc)$_2$·2H$_2$O (0.11 g, 0.50 mmol) were then added. The mixture was stirred overnight to give a yellow precipitate. The precipitate was separated by filtration, washed with light petroleum, and dried under vacuum. The crude material was dissolved in DMF (6 mL) to give an orange solution. Orange crystals of **7a**·DMF·H$_2$O were obtained by slow diffusion of Et_2O into that solution. The crystals were separated by filtration, washed with Et_2O, and dried under vacuum (yield 74 mg, 22%). IR (KBr): $\tilde{\nu}$ = 2926 w, 2855 w, 1901 vs, 1831 vs, 1663 s, 1606 s, 1582 m, 148 m, 1430 m, 1406 s, 1387 s, 1340 m, 1254 m, 1218 w, 1157 m, 1094 m, 1057 m, 1019 m, 918 w, 948 w, 889 w, 823 w, 774 m, 660 m, 611 m, 585 m, 412 m cm^{-1}. $C_{26}H_{24}MnN_5O_4Zn \cdot DMF$ (663.93): calcd. C 52.46, H 4.71, N 12.66; found C 52.08, H 4.75, N 12.59.

Complex 7b: A solution of **5b** (0.26 g, 0.50 mmol) in THF (200 mL) was irradiated with a high-pressure mercury lamp in a quartz tube at –40 °C. After about 1 h the color of the solution had changed from light yellow to yellow and the solution was allowed to warm to room temperature. KO*t*Bu (0.056 g, 0.50 mmol) and Zn(OAc)$_2$·2H$_2$0 (0.11 g, 0.50 mmol) were added and the mixture was stirred for 48 h. After removal of the solvent under reduced pressure, the residue was washed with light petroleum and dried under vacuum. Slow diffusion of Et_2O into a solution of the crude material in CH_2Cl_2 (8 mL) gradually gave orange-yellow crystals. These were separated by filtration, washed with Et_2O, and dried under vacuum (yield 57 mg, 19%). IR (KBr): $\tilde{\nu}$ = 308 w, 2975 w, 2911 w, 2850 w, 1898 vs, 1823 vs, 1607 m, 1578 m, 1483 w, 1443 m, 1416

Table 3. Crystal data and refinement details for **6a**, **6b**, **7a**, **7b**, and **8**

	6a	**6b**	**7a**·DMF·H$_2$O	**7b**	**8**
Formula	$C_{24}H_{22}MnN_5O_2$	$C_{26}H_{26}MnN_5O_2$	$C_{26}H_{24}MnN_5O_4Zn \cdot C_3H_7NO \cdot H_2O$	$C_{28}H_{28}MnN_5O_4Zn$	$[C_{26}H_{25}MnN_5O_2Zn]^+ \cdot ClO_4^-$
Mol. mass	467.41	495.46	681.95	618.88	659.29
Crystal size (mm)	0.43 × 0.38 × 0.32	0.32 × 0.23 × 0.21	0.49 × 0.12 × 0.11	0.42 × 0.34 × 0.26	0.32 × 0.19 × 0.18
Crystal system	monoclinic	monoclinic	triclinic	monoclinic	triclinic
Space group	*C*2/*c* (No. 15)	*P*2$_1$/*a* (No. 14)	*P*$\bar{1}$ (No. 2)	*P*2$_1$/*c* (No. 14)	*P*$\bar{1}$ (No. 2)
a [Å]	19.9753(12)	9.8267(7)	11.3286(12)	15.3470(12)	9.0716(8)
b [Å]	10.5765(7)	21.2521(17)	11.4389(13)	8.1298(4)	10.1812(8)
c [Å]	20.5310(15)	11.6223(8)	12.5080(16)	21.2398(17)	15.4600(12)
α [°]	90	90	91.908(10)	90	74.096(6)
β [°]	91.186(5)	111.457(5)	113.974(9)	97.390(6)	85.768(7)
γ [°]	90	90	97.228(9)	90	75.200(6)
V [Å^3]	4336.6(5)	2259.0(3)	1462.9(3)	2628.0(3)	1327.66(19)
$\rho_{calcd.}$ [g cm^{-3}]	1.432	1.457	1.548	1.564	1.649
Z	8	4	2	4	2
F_{000}	1936	1032	704	1272	672
μ(Mo-K$_\alpha$) [mm^{-1}]	0.641	0.619	1.305	1.438	1.531
T_{max}/T_{min}	0.9236/0.7724	0.8850/0.8036	0.8080/0.4746	0.7968/0.6055	0.8284/0.6161
hkl range	–21–23, ±12, –24–23	±11, ±24, ±13	±13, ±13, ±14	±18, –9–8, –24–25	–9–10, ±11, ±18
θ range [°]	1.98–24.81	1.88–24.74°	1.79–24.63	1.93–24.78°	2.15–24.80
Measured refl.	11939	10952	11941	14257	13460
Unique refl. [R_{int}]	3543 [0.0264]	3712 [0.0279]	4874 [0.0761]	4499 [0.0489]	4536 [0.0369]
Observed refl. $I > 2\sigma(I)$	3018	3180	3576	3503	3906
Refined parameters	293	311	397	353	361
Resid. electron density [e Å^{-3}]	0.281/–0.338	0.351/–0.246	0.408/–0.577	0.389/–0.534	0.478/–0.290
*R*1	0.0296	0.0310	0.0426	0.0350	0.0270
*wR*2 (all data)	0.0826	0.0786	0.0932	0.0790	0.0681
Goodness-of-fit	1.057	1.019	1.031	1.062	1.043

m, 1331 w, 1256 m, 1161 m, 1112 m, 1059 m, 1017 m, 836 w, 764 m, 664 m, 592 m, 419 w cm^{-1}. $C_{28}H_{28}MnN_5O_4Zn·0.5H_2O$ (627.89): calcd. C 53.56, H 4.66, N 11.15; found C 53.41, H 4.67, N 11.15.

Complex 8: A solution of **5b** (0.26 g, 0.50 mmol) in THF (200 mL) was irradiated with a high-pressure mercury lamp in a quartz tube at –40 °C. After about 1 h the color of the solution had changed from light yellow to yellow. It was allowed to warm to room temperature, and KO*t*Bu (0.056 g, 0.50 mmol) and $Zn(ClO_4)_2·6H_2O$ (0.185 g, 0.50 mmol) were then added. The mixture was stirred overnight to give a yellow precipitate. The precipitate was separated by filtered, washed with light petroleum, and dried under vacuum. Orange crystals were obtained after several days by slow diffusion of diethyl ether into a DMF solution (10 mL) of the crude product. The crystals were separated by filtration, washed with diethyl ether, and dried under vacuum (yield 127 mg, 39%). IR (KBr): $\tilde{\nu}$ = 3098 w, 2917 w, 2883 w, 1906 vs, 1833 vs, 1613 m, 1569 w, 1492 m, 1447 m, 1329 w, 1310 w, 1102 s, 772 m, 659 w, 624 m, 593 w, 423 w cm^{-1}. $C_{26}H_{25}ClMnN_5O_6Zn·H_2O$ (677.31): calcd. C 46.11, H 4.02, N 10.34; found C 45.33, H 3.96, N 10.29.

X-ray Crystallographic Study: X-ray data were collected on a STOE IPDS II diffractometer (graphite-monochromated Mo-K_α radiation, λ = 0.71073 Å) by use of ω scans at –140 °C (Table 3). The structures were solved by direct methods and refined on F^2, using all reflections, with SHELX-97.[24] The non-hydrogen atoms were refined anisotropically. Hydrogen atoms which were not involved in hydrogen bonding were placed in calculated positions and assigned an isotropic displacement parameter of 0.08 $Å^2$. The positional and isotropic thermal parameters of the nitrogen-bonded hydrogen atom H(2) in **6a** and **6b** were refined without constraints. A DFIX (0.83 Å) restraint was applied to the H–O distances of the H_2O molecule in **7b** and the hydrogen atoms were refined with an isotropic displacement parameter of 0.08 $Å^2$. Face-indexed absorption corrections were performed numerically with the program X-RED.[25] The geometrical aspects of the structures were analyzed with the PLATON program.[26]

CCDC-248451 (for **6a**), -248452 (for **6b**), -248453 (for **7a**·DMF·H_2O), -248454 (for **7b**), and -248455 (for **8**) contain the supplementary crystallographic data for this paper. These data can be obtained free of charge from The Cambridge Crystallographic Data Centre via www.ccdc.cam.ac.uk/data_request/cif.

Supporting Information Available (see also the footnote on the first page of this article): View of the hydrogen-bonding interactions of **7a**·DMF·H_2O (Figure S1).

Acknowledgments

Financial support by the Fonds der Chemischen Industrie is gratefully acknowledged. We sincerely thank J. Teichgräber for CV measurements and M. Alvariño Gil for preparing some of the ligand side-arms.

[1] a) J. Okuda, *Comments Inorg. Chem.* **1994**, *16*, 185–205; b) C. Müller, D. Vos, P. Jutzi, *J. Organomet. Chem.* **2000**, *600*, 127–143; c) P. Jutzi, J. Dahlhaus, *Coord. Chem. Rev.* **1994**, *137*, 179–199.

[2] a) I. L. Fedushkin, S. Dechert, H. Schumann, *Organometallics* **2000**, *19*, 4066–4076; b) L. F. Groux, F. Bélanger-Gariépy, D. Zargarian, R. Vollmerhaus, *Organometallics* **2000**, *19*, 1507–1513; c) O. Segnitz, M. Winter, K. Merz, R. A. Fischer, *Eur. J. Inorg. Chem.* **2000**, 2077–2085; d) A. I. Philippopoulos, B. Donnadieu, R. Poilblanc, N. Hadjiliadis, *J. Organomet. Chem.* **1999**, *582*, 286–291; e) H. Schumann, E. C. Rosenthal, J. Demtschuk, G. A. Molander, *Organometallics* **1998**, *17*, 5324–5333; f) P. T. Gomes, M. L. H. Green, A. M. Martins, *J. Organomet. Chem.* **1998**, *551*, 133–138; g) P. Foster, J. C. W. Chien, M. D. Rausch, *J. Organomet. Chem.* **1997**, *545–546*, 35–38; h) Z. Ziniuk, I. Goldberg, M. Kol, *J. Organomet. Chem.* **1997**, *545–546*, 441–446; i) P.-J. Sinnema, L. van der Veen, A. L. Spek, N. Veldman, J. H. Teuben, *Organometallics* **1997**, *16*, 4245–4247; j) A. K. Hughes, J. A. Kingsley, *J. Chem. Soc., Dalton Trans.* **1997**, 4139–4142; k) M. Enders, R. Rudolph, H. Pritzkow, *Chem. Ber.* **1996**, *129*, 459–463; l) W. A. Herrmann, M. J. A. Morawietz, T. Priermeier, K. J. Mashima, *J. Organomet. Chem.* **1995**, *486*, 291–295.

[3] a) U. Siemeling, P. Jutzi, *J. Organomet. Chem.* **1995**, *500*, 175–185; b) P. Jutzi, T. Redeker, *Eur. J. Inorg. Chem.* **1998**, 663–674.

[4] a) P. J. Shapiro, E. Bunel, W. P. Schaefer, J. E. Bercaw, *Organometallics* **1990**, *9*, 867–869; b) A. L. McKnight, R. M. Waymouth, *Chem. Rev.* **1998**, *98*, 2587–2598 and references cited therein; c) R. Emrich, O. Heinemann, P. W. Jolly, C. Krüger, G. P. J. Verhovnik, *Organometallics* **1997**, *16*, 1511–1513; d) M. S. Blais, J. C. W. Chien, M. D. Rausch, *Organometallics* **1998**, *17*, 3775–3783; e) K. C. Hultzsch, T. P. Spaniol, J. Okuda, *Angew. Chem.* **1999**, *111*, 163–165; *Angew. Chem. Int. Ed.* **1999**, *38*, 227–230; f) P. T. Witte, A. Meetsma, B. Hessen, *Organometallics* **1999**, *18*, 2944–2946.

[5] J. C. Röder, F. Meyer, H. Pritzkow, *Organometallics* **2001**, *20*, 811–817.

[6] a) J. C. Röder, F. Meyer, E. Kaifer, *Angew. Chem.* **2002**, *114*, 2414–2417; *Angew. Chem. Int. Ed.* **2002**, *41*, 2304–2306; b) J. C. Röder, F. Meyer, I. Hyla-Kryspin, R. F. Winter, E. Kaifer, *Chem. Eur. J.* **2003**, *9*, 2636–2648.

[7] J. C. Röder, F. Meyer, R. F. Winter, E. Kaifer, *J. Organomet. Chem.* **2002**, *641*, 113–120.

[8] a) C. J. Qin, A. L. Gavrilova, B. Bosnich, *Pure Appl. Chem.* **2001**, *73*, 221–226; b) A. L. Gavrilova, B. Bosnich, *Inorg. Chim. Acta* **2003**, *352*, 24–30.

[9] K. G. Caulton, *Coord. Chem. Rev.* **1981**, *38*, 1–43.

[10] W. Kaim, R. Gross, *Comments Inorg. Chem.* **1988**, *7*, 269–285.

[11] T. G. Schenck, C. R. C. Milne, J. F. Sawyer, B. Bosnich, *Inorg. Chem.* **1985**, *24*, 2338–2344.

[12] Photolability of one CO ligand in $[CpMn(CO)_3]$ and its derivatives is well established: a) W. Strohmeier, *Angew. Chem.* **1964**, *76*, 873–881; *Angew. Chem. Int. Ed. Engl.* **1964**, *3*, 730–738; b) W. Strohmeier, F.-J. Müller, *Chem. Ber.* **1969**, *102*, 3608–3612.

[13] a) N. C. Mösch-Zanetti, M. Ferbinteanu, J. Magull, *Eur. J. Inorg. Chem.* **2002**, 950–956; b) G. B. Deacon, C. M. Forsyth, A. Gitlits, R. Harika, P. C. Junk, B. W. Skelton, A. H. White, *Angew. Chem.* **2002**, *114*, 3383–3385; *Angew. Chem. Int. Ed.* **2002**, *41*, 3249–3251; c) J. Hitzbleck, A. Y. O'Brien, C. M. Forsyth, G. B. Deacon, K. Ruhlandt-Senge, *Chem. Eur. J.* **2004**, *10*, 3315–3323.

[14] The degree of trigonality can be evaluated by means of the angular structural parameter $\tau = (\beta - \alpha)/60$, where α and β represent the two largest angles around the central atom with $\beta > \alpha$ (a perfect TB-5 structure is associated with τ = 1, while τ = 0 is expected for ideal SPY-5 geometry): A. W. Addison, T. N. Rao, J. Reedijk, J. van Rijn, G. C. Verschoor, *J. Chem. Soc., Dalton Trans.* **1984**, 1349–1356.

[15] H. Adams, N. A. Bailey, D. A. Fenton, Q.-Y. He, *J. Chem. Soc., Dalton Trans.* **1997**, 1533–1540.

[16] G. B. Deacon, R. J. Phillips, *Coord. Chem. Rev.* **1980**, *33*, 227–250.

[17] X. Xu, C. S. Allen, C.-L. Chuang, J. W. Canary, *Acta Crystallogr., Sect. C* **1998**, *54*, 600–601.

[18] An unusual side-on π-interaction has been observed for a nitrile moiety within the bimetallic pocket of a pyrazolate-based dinickel(II) complex, with Ni–N and Ni–C distances around 2.9 Å: F. Meyer, I. Hyla-Kryspin, E. Kaifer, P. Kircher, *Eur. J. Inorg. Chem.* **2000**, 771–781.

[19] R. Gross, W. Kaim, *Angew. Chem.* **1985**, *97*, 869–870; *Angew. Chem. Int. Ed. Engl.* **1985**, *24*, 856–858.
[20] I. A. Veselov, V. G. Shtyrlin, V. A. Zakharov, *Koord. Khim. (Koordinatsionnaya Khimiya; Russ. J. Coord. Chem.)* **1988**, *14*, 943–947.
[21] Departures from first-order line-spacings result from coincidence of the *x* and z principal axes of the *g* and ^{55}Mn hyperfine tensors: R. D. Pike, A. L. Rieger, P. H. Rieger, *J. Chem. Soc., Faraday Trans. 1* **1989**, *85*, 3913–3925.
[22] *Spartan 02*, Wavefunction Inc.: Irvine, CA. The UB3LYP method with the LACVP* basis set was employed. Geometry optimization was started from the coordinates obtained from the X-ray structure of **8**. A doublet ground state was applied as the only constraint.
[23] N. G. Connelly, W. E. Geiger, *Chem. Rev.* **1996**, *96*, 877–910.
[24] G. M. Sheldrick, *SHELXL-97*, Program for Crystal Structure Refinement, Universität Göttingen, **1997**. G. M. Sheldrick, *SHELXS-97*, Program for Crystal Structure Solution, University of Göttingen, **1997**.
[25] STOE & CIE GmbH, *X-RED*, Darmstadt, **2002**.
[26] A. L. Spek, *PLATON*, A Multipurpose Crystallographic Tool, Utrecht University, **2003**.

Received: August 25, 2004

